Science Advances

AAAS

advances.sciencemag.org/cgi/content/full/3/9/e1701471/DC1

Supplementary Materials for

Water on the surface of the Moon as seen by the Moon Mineralogy Mapper: Distribution, abundance, and origins

Shuai Li and Ralph E. Milliken

Published 13 September 2017, *Sci. Adv.* **3**, e1701471 (2017)
DOI: 10.1126/sciadv.1701471

This PDF file includes:

Supplementary Text

Reflectance spectra were measured for a series of synthetic hydrated basaltic glasses (lunar compositions), terrestrial volcanic glasses, and a terrestrial anorthosite. Different particle size ranges and water contents were examined to determine relevant ESPAT-%H_2O trends and to examine how these factors affect these trends, and the detailed methodology and results are presented in (*38*).

Reflectance spectra for each sample were measured in the NASA Reflectance Experiment LABoratory (RELAB) facility at Brown University using a Nicolet FTIR over a wavelength range of ~1-25 μm. Samples were measured under continuous flow of dry air (scrubbed for CO_2, dew point of ~70°C). All reflectance spectra were converted to single scattering albedo (SSA) spectra using Hapke theory, and the resulting SSA spectra were then used to determine ESPAT values for the water absorptions at a wavelength of ~2.9 μm.

A sample of terrestrial anorthosite from Timmons, Ontario, provided by Dr. Ralph Milliken (Brown University), was ground and sieved to <45 μm. Sample weight and reflectance spectra were recorded at ambient temperature, after 20 minutes of purging in dry air, and after heating from 100-600°C in 50 °C increments for 30 minutes at each step. Sample weight and spectra (fig. S8) were measured immediately after each heating step to avoid contamination from atmospheric water.

The anorthosite sample was contaminated by organic matter showing an absorption at ~3.4 μm (fig. S8, black arrow) due to C-H vibrations, which can affect the apparent strength of water absorptions in the 3 μm region as well as measured weight losses. Thus, only one particle size group (< 45 μm) was used to examine the ESPAT-%H_2O trend. To account for the contribution of organics we assume that ESPAT values for organic bands at ~3.4 μm are, like water, linearly correlated to abundance. ESPAT values for the organic contribution, E_o, can thus be related to organic content, W_o, by $W_o\% = a_o E_o$, where a_o is the slope. Similarly, ESPAT of the water contribution, E_w, can be related to water content, W_w, by $W_w\% = a_w E_w$ (*26, 46, 54, 55*). The total weight loss after each step of heating is defined as $W_{loss}\% = W_o\% + W_w\%$, which can be rewritten as $a_o E_o + a_w E_w = W_{loss}\%$. In matrix form, $EA_{ow} = W$, where

$$E = \begin{bmatrix} E_{o1} & E_{w1} \\ E_{o2} & E_{w2} \\ \bullet & \bullet \\ E_{on} & E_{wn} \end{bmatrix},\ A_{ow} = \begin{bmatrix} a_o \\ a_w \end{bmatrix},\ W = \begin{bmatrix} W_1 \\ W_2 \\ \bullet \\ W_n \end{bmatrix}$$

The values for E_o *and* E_w are calculated from SSA spectra at ~3.4 and ~2.9 μm, respectively, corresponding to each step of the heating experiments. The two unknowns, a_o and a_w, are then estimated using a least-squares approach: $A_{ow} = (E'E)^{-1}E'W$. This yields a value of a_w = 1.8 that can be used to predict water content based on ESPAT values for this sample.

A suite of Middle Ocean Ridge Basalt (MORB) glasses were provided by Dr. Alberto Saal (Brown University) to assess ESPAT-%H_2O trends to explore volcanic samples with a wider range in water content than present in the synthetic lunar glasses. Criteria for selection of these samples included i) water contents less than 20,000 ppm (2 wt.%), which is an appropriate range for lunar materials, and ii) samples should be as visually homogeneous and free of alteration products as possible. A total of four samples were examined, all of which were previously measured with SIMS to determine absolute water content (*58*). The sample information and their water contents can be found in (*38*). These samples were sieved to particle size ranges of <45μm, 32-53μm, 63-75μm, and 106-125μm to examine ESPAT-%H_2O trends as a function of particle size and for comparison to the numerical ESPAT-%H_2O simulations. Stepwise heating experiments similar to what was done for the anorthosite were only carried out for one sample D38A because the water content for other samples was low enough that the weight loss for each step is less than 10^{-4} g out of the detection limit of the scale in the laboratory. No correction for organic contaminants for sample D38A was necessary. Spectra for these samples are shown in fig. S9.

Supplementary Figures

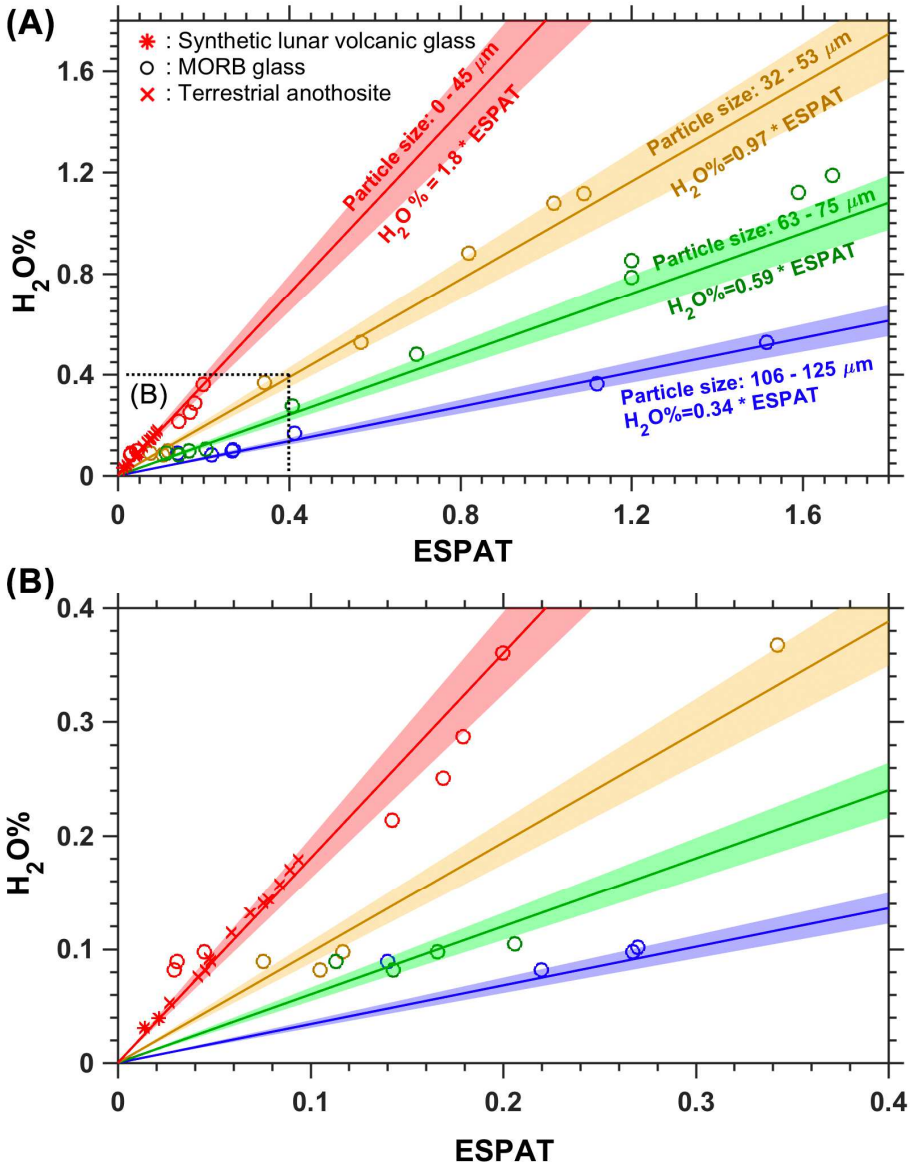

fig. S1. The linear trends between ESPAT and weight % H_2O for materials typifying the lunar surface. (**A**) The ESPAT-%H_2O trends derived from laboratory experiments and simulations (solid lines, shaded regions show uncertainties) for lunar-relevant compositions and particle sizes; (**B**) A zoomed-in view of the area outlined by dashed lines in (A), full details as to how these data are measured/derived can be found in (*38*), modified from Fig. 2-2 in (*38*).

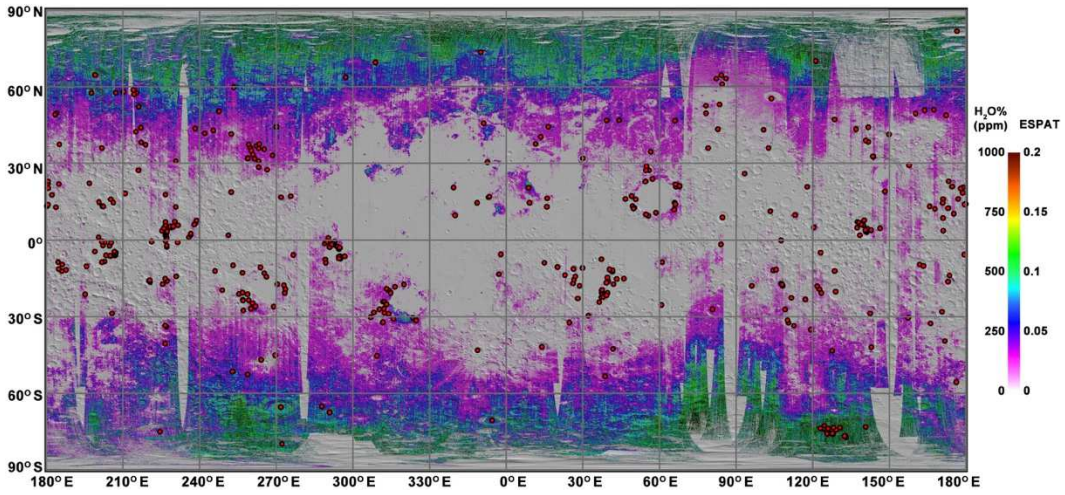

fig. S2. Crystalline plagioclase exposures identified in the M³ data by Donaldson Hanna *et al.* (*36*) overlain on map of lunar surface water derived from the M³ data.

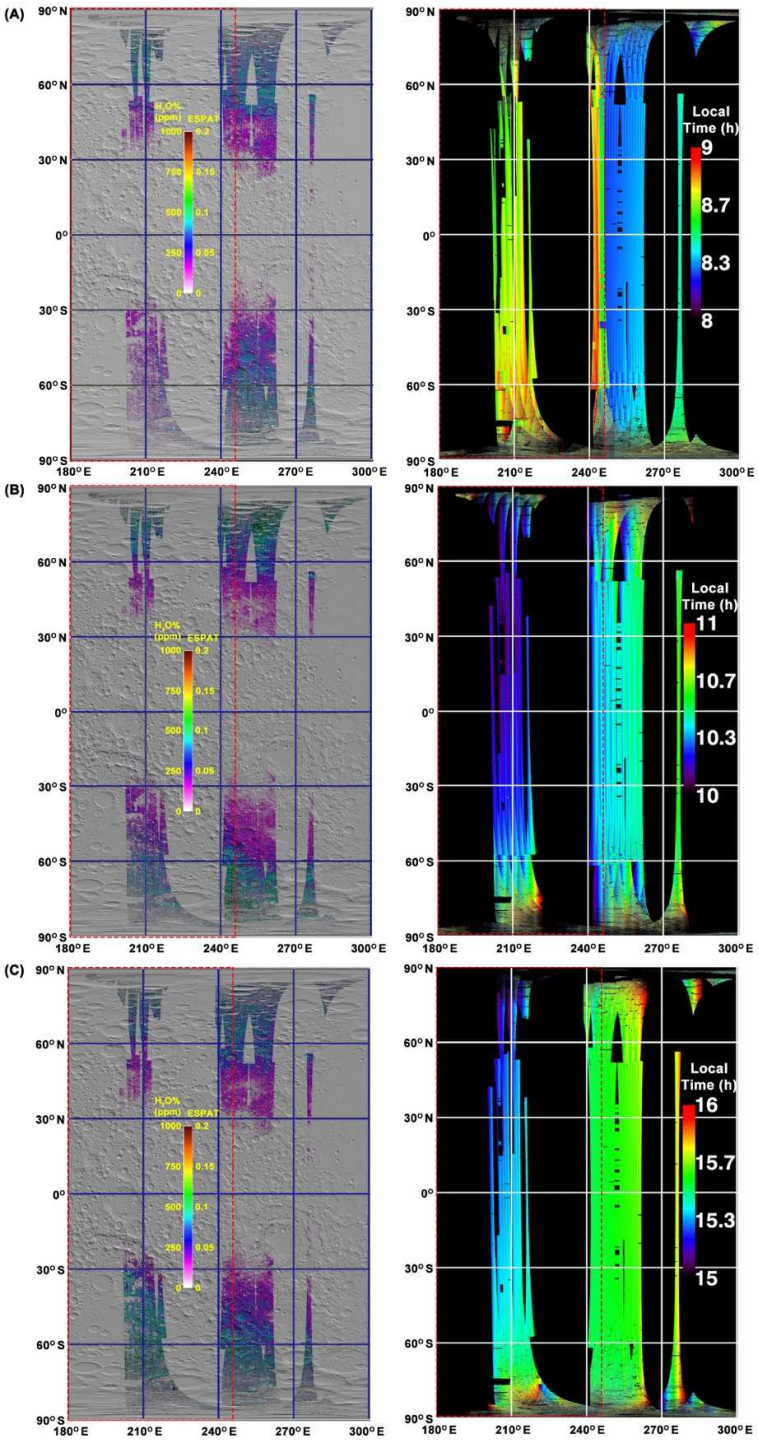

fig. S3. The water content (ESPAT) mapped by M³ at three different lunar local time and the respective acquisition time of M³ data. Mosaic of ESPAT/water content map (assuming 60 – 80 μm particle size; left column) and map of respective local hours (right column) from M³ data acquired (**A**) during local morning, (**B**) near local noon, and (**C**) during local afternoon. Data outlined by the red dashed lines were not used in assessing the diurnal variation of lunar surface water (see text for details).

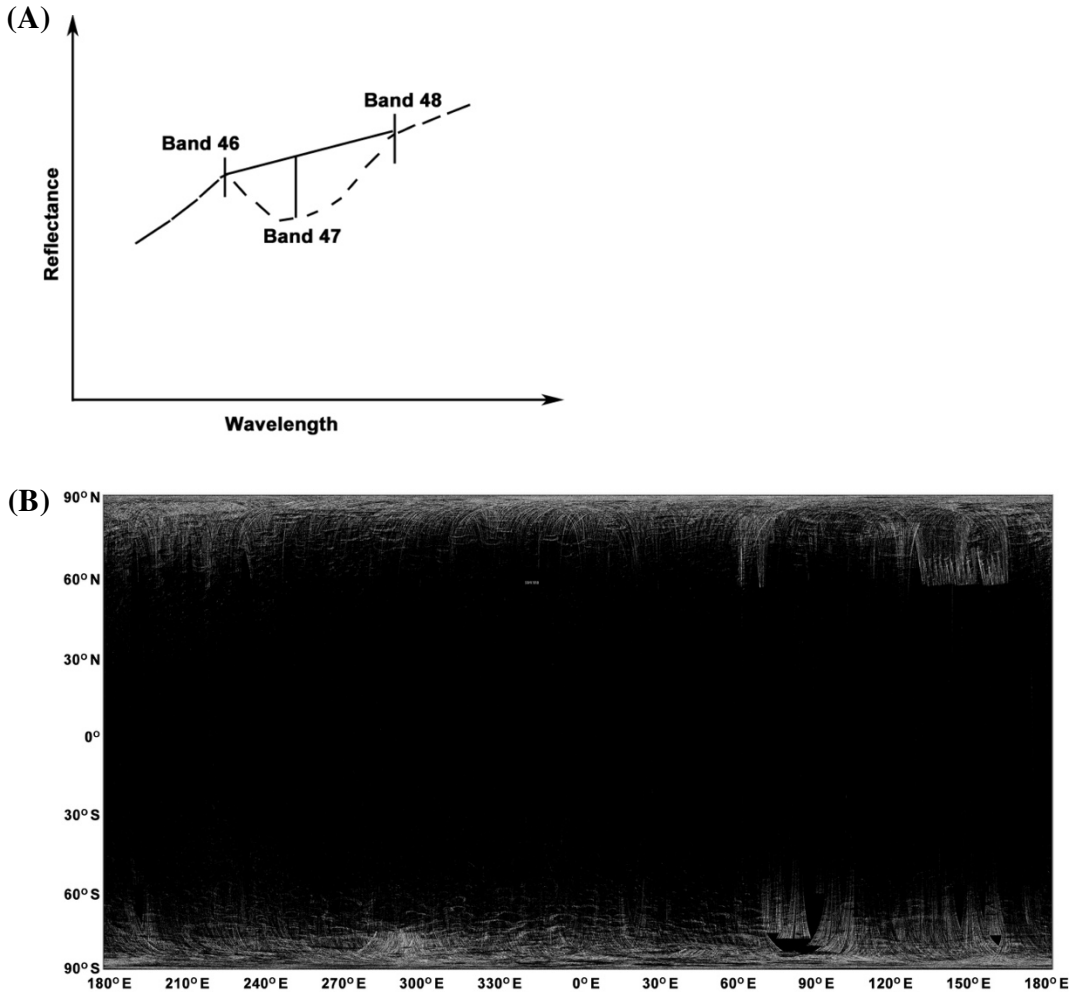

fig. S4. **Filtering of the M^3 data due to spectral artifacts affecting bands 47 and 74.** (**A**), Schematic plot illustrating erratic decrease in reflectance at band 47 in some M^3 data; similar effects occur at band 74 in some pixels. (**B**), Map of M^3 pixels that are masked (white tones) due to artifacts at band 47 or 74 that are above our defined threshold; most masked pixels occur at high latitudes where signal at detector is low due to poor illumination.

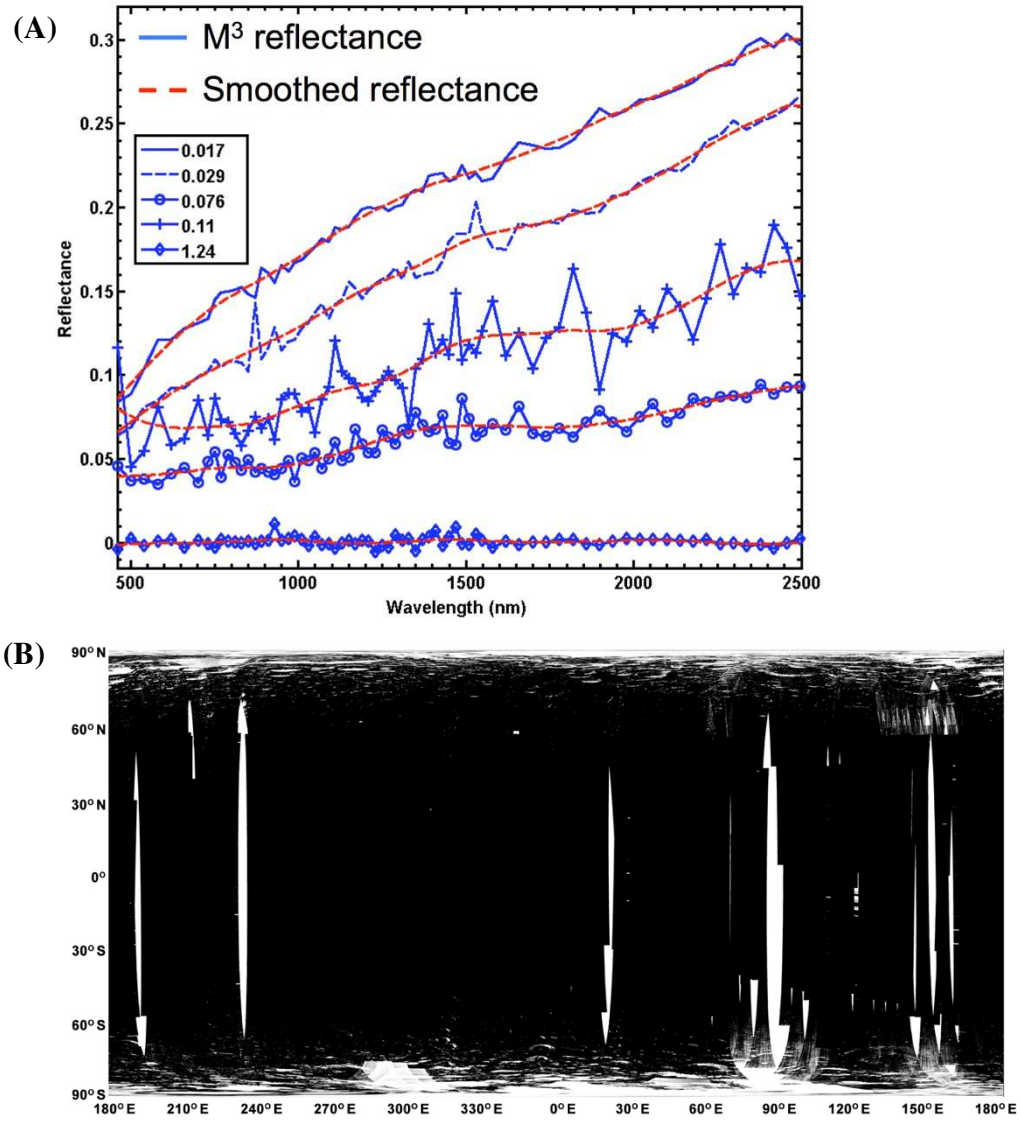

fig. S5. Filtering of the M³ data by SNRI (see Methods for details). (**A**), Example spectra with different SNRI values, from low to high, and (**B**), map of M³ pixels that are masked (white tones) due to low SNRI values. Note that pixels with SNRI > 0.1 are masked and primarily occur at high latitudes.

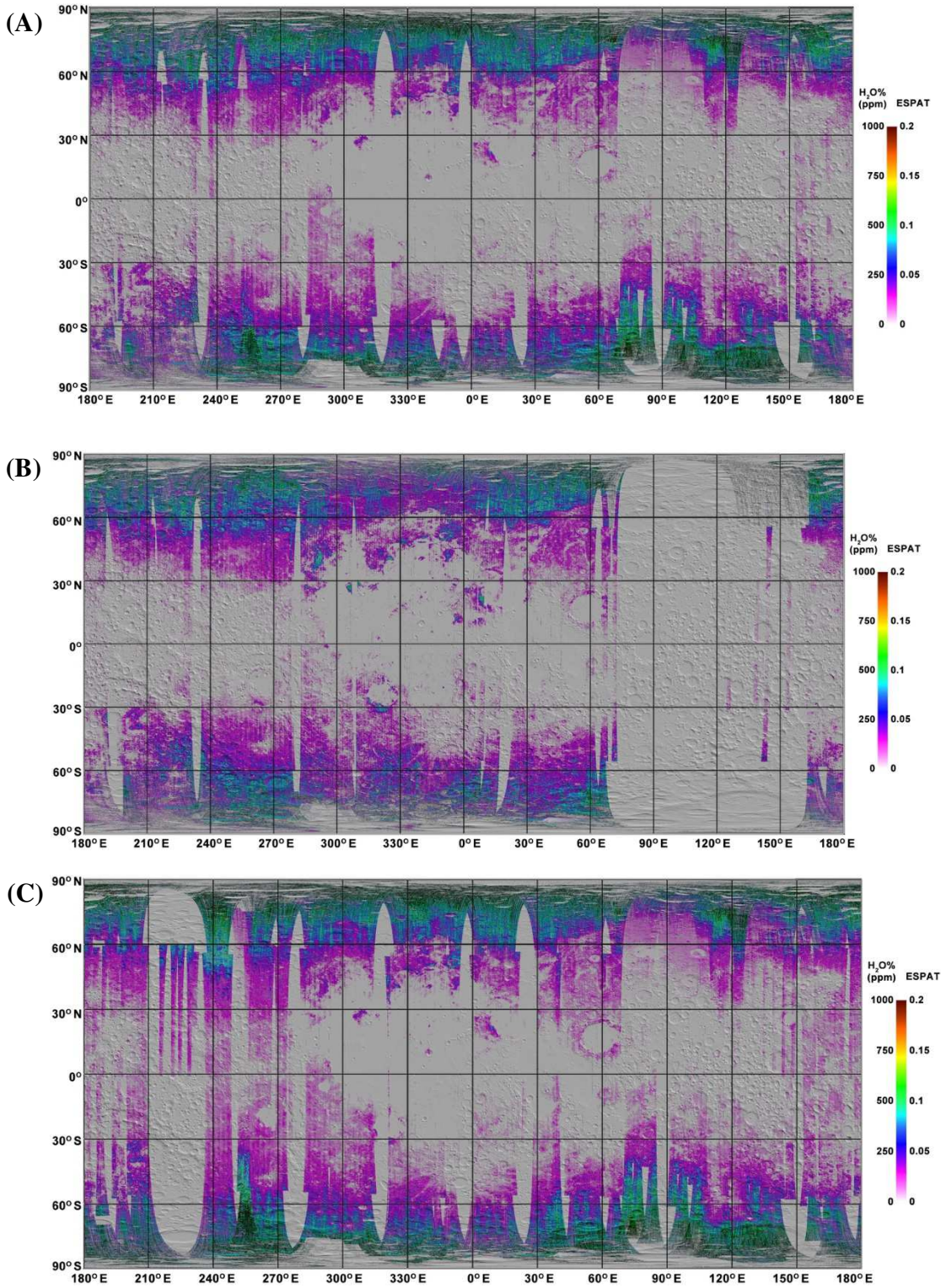

fig. S6. The global water map (ESPAT) of OP2C and maps acquired at different sensor temperatures. Mapped lunar surface ESPAT/water (assuming 60-80 μm particle size) with images acquired (**A**) during optical period (OP2C) with the best spatial coverage, (**B**) when detector was 'cold'(*51*), and (**C**) when detector was 'hot'(*51*).

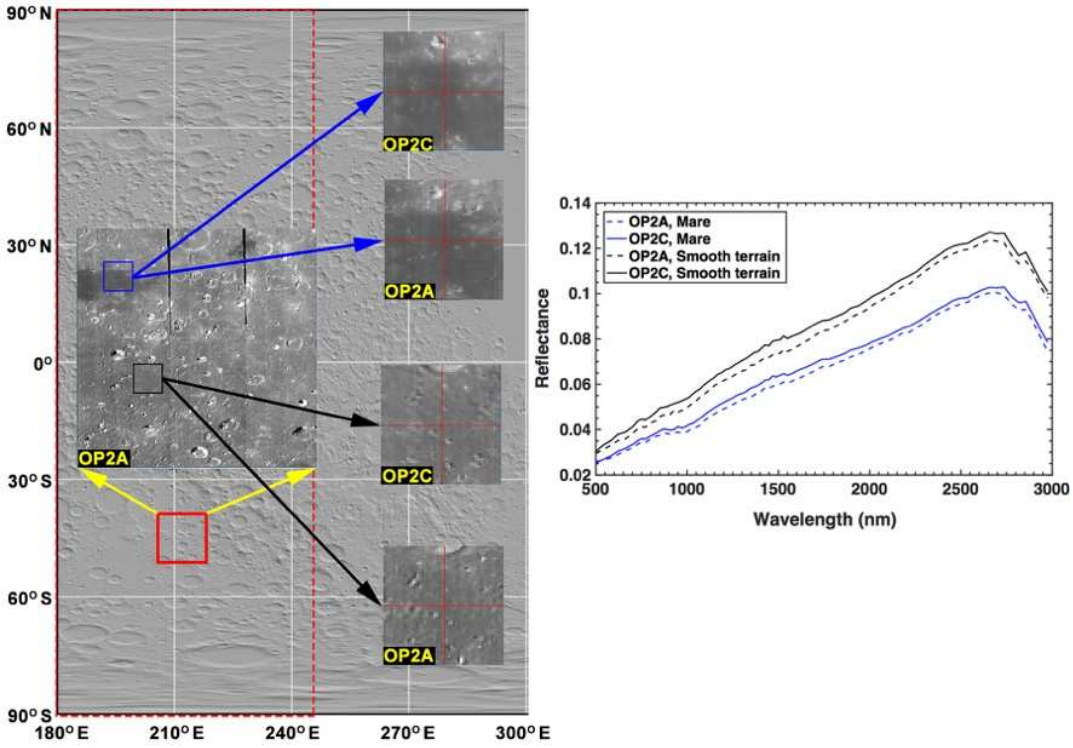

fig. S7. Examples of spectral discrepancies (overall reflectance level and spectral slope) between the M³ OP2A and OP2C data sets.

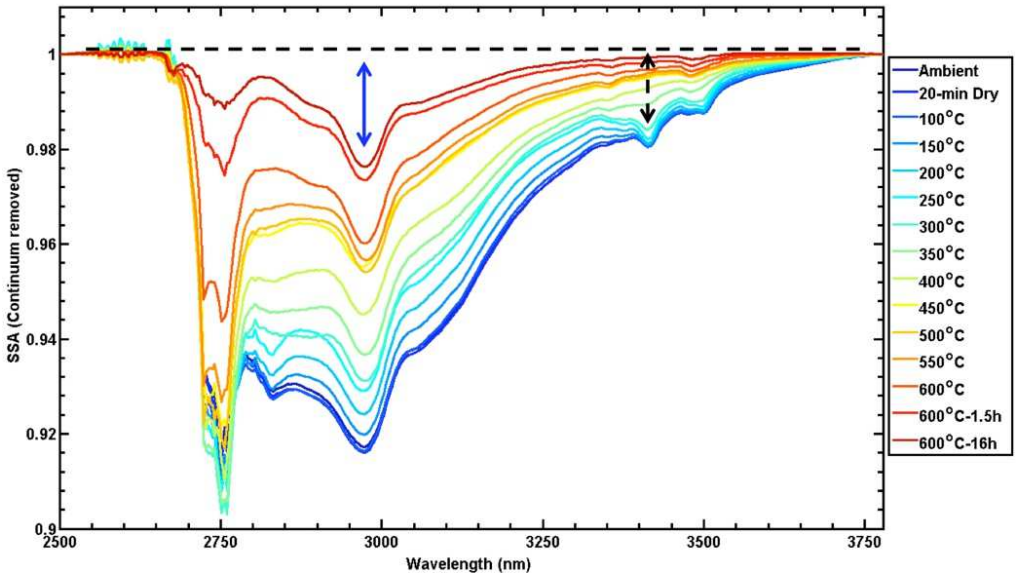

fig. S8. SSA spectra of anorthosite after continuum removal over the 2.5-µm to 3.8-µm-wavelength region for data acquired from results during the stepwise heating experiments. The blue arrow indicates a fundamental water absorption whereas the black arrow indicates C-H absorptions due to organic compounds.

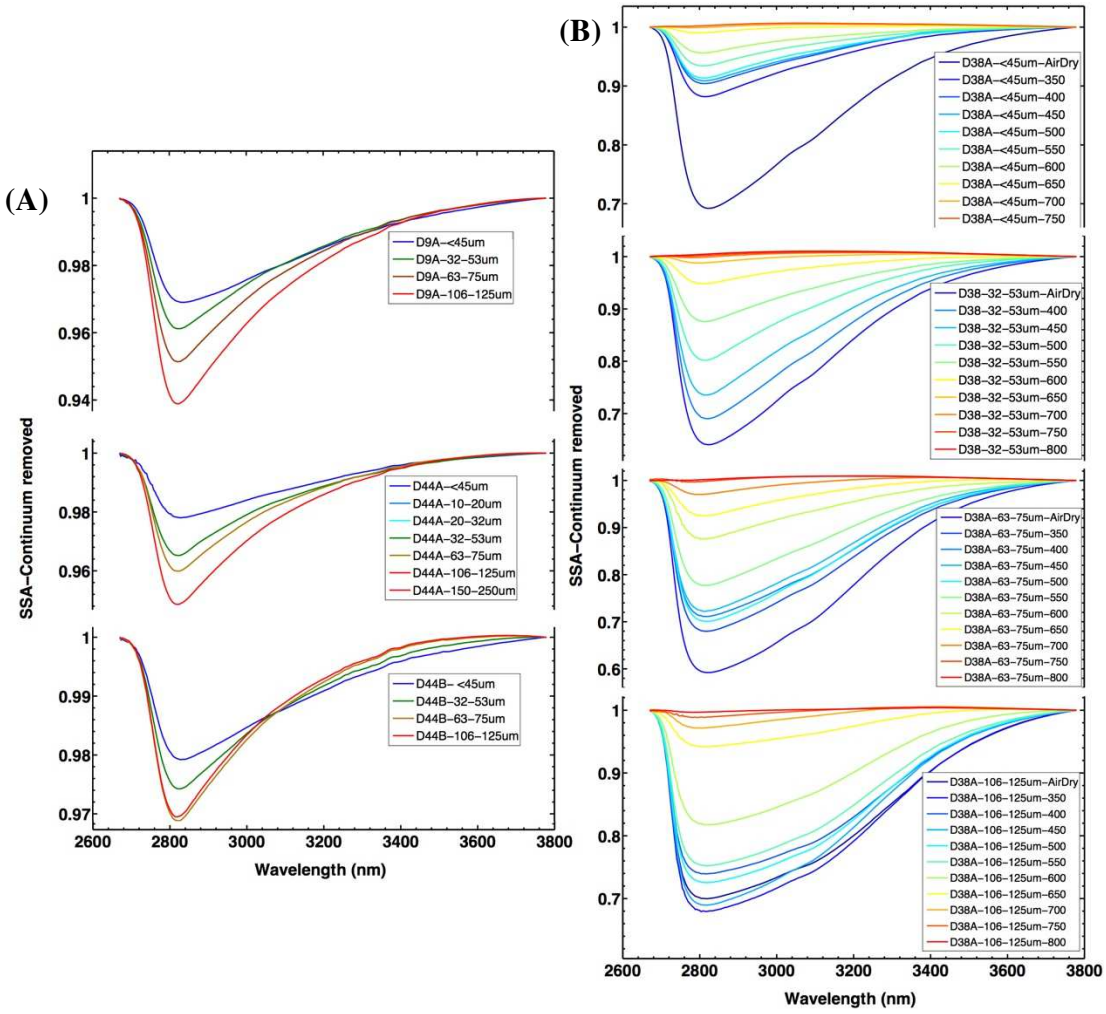

fig. S9. Continuum-removed reflectance spectra of MORB glass samples. Continuum-removed reflectance spectra of MORB glass samples for (**A**) four particle size groups for 3 samples and (**B**) for stepwise heating experiments for four particle size groups for sample D38A.

Supplementary Tables

table S1. Results from select pyrolysis measurements that were performed on lunar regolith, mineral separates, agglutinates, and rocks sampled from the Apollo 11, 12, 14, 15, 16, and 17 landing sites. Only water amounts measured from temperatures above 300°C are listed and used for Fig. 2 in order to minimize potential effects of terrestrially adsorbed water.

Reference	Sample Name	H_2O (ppm)	δD (‰)	Temperature
Merlivat *et al.*, 1974 (*59*)	15600 regolith	46.8	-59	>600°
	15600 regolith	68.4	-95	
	68501 regolith	93.6	-115	
	72501 regolith	90	-88	
	72501 regolith	82.8	-82	
	78501 regolith	104.4	-72	
	15229 agglutinate	228.6	-52	
	15229 agglutinate	7.2	-242	
	70215 basalt	48.6	-165	
	75035 basalt	44.6	-92	
	75035 basalt	50.4	-252	
Epstein and Taylor, 1973 (*60*)	15021.4 regolith	48.6	-252	630°-melting
	64421.21 regolith	109.8	-280	500°-melting
	65513.1 regolith	268.2	-173	500°-melting
	62221.8 regolith	199.8	-88	500°-melting
	74220.22 regolith	46.8	-154	500°-melting
Friedman *et al.*, 1971 (*61*)	12030.30 regolith	7	-300	430°-1025°
Friedman *et al.*, 1970 (*62*)	10046.21 agglutinate	455	-756	300°-950°
	10046.22 agglutinate	372	-576	300°-950°
	10060.11 agglutinate	152	-865	300°-950°
Epstein and Taylor, 1970 (*3*)	10084.2 rock and minerals	90.4	-380	500°-1400°
	10084.1 rock and minerals	208.4	-268	500°-1400°
	10061 rock and minerals	160.2	-409	500°-1400°
Epstein and Taylor, 1972 (*63*)	14422 regolith	48.6	-419	550°-600°
Friedman *et al.*, 1974 (*64*)	66095.62 rock	9	-194	690°-1350°
	66095.31 rock	13.5	-153	690°-1350°

table S2. SIMS measurements of water content (and δD values) for select Apollo samples that were used to generate Fig. 2.

Sample Name	H_2O (ppm)	δD (‰)	Reference
10084 Agglutinate	470	4555	Liu *et al.*, 2012
	27	5413	
	225	-562	
	282	-789	
	246	-843	
	161	-731	
	188	191	
	207	267	
70051 Agglutinate	200	-711	
	209	-844	
	203	-781	
64501 Agglutinate	79	-558	
74220 Glass	5.0	446	Saal *et al.*, 2013
	3.5	194	
	4.6	283	
	5.5	412	
	4.6	453	
	4.9	291	
	4.4	235	
	3.8	416	
	3.2	269	
	8.7	392	
	6.7	299	
	5.7	330	
	3.7	406	
	3.1	396	
	3.5	307	
15426 Low Ti glass	69.3	474	
	51.9	347	
	40.7	349	
	39.2	459	
	34.8	804	
	32.7	2199	
	30.8	2258	
	28.1	843	
	27.9	545	
	27.8	2244	
	25.1	502	
	22.8	469	
	22.0	1210	
	16.8	2160	
	16.3	580	
15427 Very Low Ti glass	33.8	578	
	28.6	1802	
	14.4	4045	
	12.1	1043	
	11.4	830	
	10.8	209	
	9.4	761	
	9.1	1028	
	8.7	616	
	7.4	80	
	6.9	371	
	6.4	-378	
	6.2	487	
	6.1	626	
	6.1	2	

	5.7	-616	
	5.6	-93	
	5.5	-119	
	5.5	-213	
	5.5	-139	
	5.3	318	
	5.3	837	
	5.3	50	
	5.1	523	
	4.9	273	
	4.4	-338	
	4.4	-165	
	4.2	2209	
	4.1	-733	
	3.6	-651	